Mechanistic and Energetic Details of Adduct Formation and σ-Bond Activation in $Zr^+(H_2)_n$ Clusters†

John E. Bushnell, Paul R. Kemper, Petra van Koppen, and Michael T. Bowers*

Department of Chemistry and Biochemistry, University of California, Santa Barbara, California 93106-9510

Received: August 23, 2000; In Final Form: October 9, 2000

The formation of $Zr^+(H_2)_n$ clusters ($n = 1-7$) has been studied both experimentally and theoretically. Binding energies were determined via temperature-dependent equilibrium measurements, giving $-\Delta H_0° = 14.5 \pm 0.3$, 10.7 ± 0.2, 10.1 ± 0.3, 9.1 ± 0.5, 9.2 ± 0.5, 8.9 ± 0.6, and 8.5 ± 0.8 kcal/mol for $n = 1-7$, respectively. Both DFT(B3LYP) and MP2 calculations gave binding energies in excellent agreement with experiment. Zr^+ appears to insert into the first H_2 to form the dihydride as predicted by theory. The rate of insertion was observed to have a negative temperature dependence and a positive pressure dependence, suggesting a cluster-assisted insertion mechanism. Interestingly, both DFT and MP2 calculations suggest that the dihydride may "uninsert" to form a pure dihydrogen cluster with n between 5 and 7.

Introduction

Different aspects of the interaction of H_2 with transition metals have received considerable attention over the past decade. Many investigations have centered on coordinately saturated organometallic compounds since the discovery of long-lived complexes containing an intact dihydrogen ligand (in contrast to a "classical" hydride).[1] These compounds are precursors to oxidative addition, an extremely important step in the catalytic reactions of hydrocarbons at transition-metal centers. In fact, many of these "nonclassical" dihydrogen-containing compounds exist in a form intermediate between one with H_2 bound as an intact dihydrogen ligand and that of a fully activated dihydride.[2−4] While this is clearly an important class of compounds for study, there are difficulties in obtaining data due to the limited number of dihydrogen-containing compounds that can be synthesized, and their unstable nature.

In this laboratory, we have examined the interaction of H_2 with a variety of transition-metal cations[5−13] using mass-spectrometric methods. We have also investigated closed-shell alkali-metal ions for comparison,[14] along with the interaction of H_2 with main-group cations.[15,16] By measuring successive $M^+(H_2)_n/M^+(H_2)_{n-1}$ equilibria in a high-pressure, variable-temperature drift/reaction cell, we have been able to accurately determine the successive enthalpies and entropies of binding of up to seven H_2 molecules to a transition-metal ion. These measurements have revealed surprising dependencies of $\Delta H°$ and $\Delta S°$ on the number of H_2 ligands coordinated to a given metal center. These variations have stimulated the application of ab initio[17−22] and density-functional techniques to these species, generating information as to their structures and energetics, which ultimately leads to a much greater understanding of the most important aspects of the interactions between different transition-metal ions and dihydrogen. This synergism between experiment and theory provides surprises and insights for both. For instance, both theory and experiment suggested that the insertion of Sc^+ into H_2 to form the dihydride was exothermic. No reaction was seen experimentally under single-collision conditions however,[23] a result explained by theory, which predicted a large barrier to reaction. In apparent contradiction to this, we found experimentally that the reaction did occur at thermal energies under multiple-collision conditions. Even more surprising, the reaction rate displayed a negative temperature dependence, a result inconsistent with a large reaction barrier. We explained this unusual behavior with a cluster-assisted activation process in which ligation by H_2 effectively lowers the insertion barrier to form the dihydride.[5] We will see below that theory can provide some surprises of its own.

In this paper we present results on the binding of up to seven hydrogen molecules to the second-row transition-metal zirconium ion, Zr^+. This is an interesting system for several reasons. First, now that we have results for the entire first-row transition-metal ions,[5−13] it is interesting to see how the general concepts learned from first-row transition-metal ion systems will transfer to the second-row metal ions. The second-row transition-metal ions differ from the first-row ions in several important ways: First, the second-row ions are larger, they have lower d−d exchange energy, and the size difference between the 5s and 4d orbitals is smaller than that between the 4s and 3d orbitals.[24,25] Further, the reactivity of transition metals is known to increase in moving from the first row to the second and third rows. For example, under single-collision conditions, all first-row $M^+ + CH_4$ reaction channels have been experimentally determined to be endothermic,[26] a result consistent with theory.[27] In the second row, only Zr^+ is observed to dehydrogenate methane at thermal energy under single-collision conditions,[28] while oligomerization is observed for third-row transition-metal ions reacting with methane.[29]

Activation of the H−H bond is thought to be easier than that of the C−H bond of CH_4 due to the more directional sp^3 bonding in methane,[30] and we might expect Zr^+ to be capable of reacting with H_2 to form the dihydride. One of the goals of this study is to determine whether Zr^+ does in fact insert into the H−H bond, and, if so, determine the rate and temperature dependence of the insertion to elucidate the mechanism of σ-bond activation in this system.

In addition to experimental results, we present results of density functional (B3LYP) and MP2 calculations of the energies and possible structures of $Zr^+(H_2)_n$. These results help one to understand the experimentally observed trends and aid

† Part of the special issue "Aron Kuppermann Festschrift".

10.1021/jp003035u CCC: $20.00 © 2001 American Chemical Society
Published on Web 12/23/2000

in the data analysis. We considered clusters where all of the H_2 ligands remain noninserted dihydrogen as well as clusters in which the Zr^+ has inserted into one H_2 to form a dihydride. Insertion into two or more H_2 ligands is very unlikely as Zr^+ contains only three valence electrons.

Experimental Method

The instruments[7,31] as well as the equilibrium[32] and kinetic experiments[5] have been described previously. Sources of error have also been discussed extensively.[8] An overview is given here with an emphasis on the differences between these experiments and those previously reported.

Instruments. Zr^+ ions were formed via surface ionization of ZrF_4 on a hot filament (both tungsten wire and 0.0015 in. rhenium ribbon were used, T∼2500K). ZrF_4 vapor was produced by heating a small sample of solid ZrF_4 in a small oven attached to the ion source. In the equilibrium measurements, ions formed in the source were accelerated to 5 keV, mass selected with a double-focusing, reverse geometry mass spectrometer, decelerated to about 5 eV, and injected into a reaction cell containing H_2 at a concentration of about 1×10^{17} molecules/cm^3 (3 Torr at 300 K). More recent kinetic measurements were performed using a similar instrument that utilizes a quadrupole for the initial mass selection. Within the reaction cell, ions are quickly thermalized via collisions with H_2, and traverse the reaction cell (4 cm in length) under the influence of a small, uniform electric field. The electric field is kept small enough that the ion thermal energy is not significantly perturbed. The H_2 pressure in the reaction cell is monitored directly using a capacitance manometer. The cell temperature is varied using a flow of heated or cooled N_2 or with electric heaters, and measured using both a thin-film platinum resistor suspended in the bath gas and multiple thermocouples attached to the cell. Ions exiting the cell are accelerated slightly (to about 5 eV), quadrupole mass analyzed, and collected using standard ion-counting techniques. The quadrupole is computer scanned over the mass range of interest, and the baseline-resolved peaks are integrated to give the relative ion intensities.

Equilibrium Experiment. After the temperature and H_2 pressure in the reaction cell have stabilized, product/parent ion ratios are measured as a function of reaction time (∝1/drift field). As the reaction time is increased, product/parent ion ratios become constant, indicating that equilibrium has been reached. While as long as 500 μs (roughly 85 000 collisions) was required for the first cluster to reach equilibrium (that is, for the ZrH_2^+/Zr^+ ratio to become constant), all subsequent clusters reached equilibrium on a time scale too short to measure in this experiment (≪100 μs). For selected experiments, the pressure of H_2 was varied by a factor of 2 with no significant change observed in the equilibrium constant.

Product/parent ion ratios are converted to equilibrium constants using eq 1, where $P_{H2}°$ is the hydrogen pressure in atmospheres. The free energy of reaction is then given by eq 2,

$$K_P° = \frac{[Zr^+(H_2)_n]}{[Zr^+(H_2)_{n-1}]} \frac{1}{P_{H2}°} \quad (1)$$

where R is the gas constant and T is the temperature. Over the

$$\Delta G° = -RT \ \ln(K_P°) \quad (2)$$

experimental temperature range, a plot of $\Delta G°$ vs temperature is essentially linear with a slope equal to $-\Delta S_T°$ and intercept of $\Delta H_T°$ (T is the average experimental temperature). Plotting the data in this way is functionally equivalent to the more common van't Hoff plot, but is more convenient for our data analysis (described below).

Analysis of the equilibrium data involves extracting the value of $\Delta H_0°$, the binding energy at 0 K, which is a more fundamental quantity than $\Delta H_T°$. We do this by calculating $\Delta G°$ vs temperature using statistical mechanics and then matching the experimental and theoretical plots. While this procedure requires a variety of parameters (rotational constants, vibrational frequencies, etc.), these parameters are usually known with sufficient accuracy to make $\Delta H_0°$ the only significant variable and thus give a very well determined value for $\Delta H_0°$. In other words, the data analysis is not sensitive to reasonable errors in the calculated rotational constants and vibrational frequencies. These input parameters are varied over a wide range, and the resulting variation in $\Delta H_0°$ is included in the reported error limits.

We must also consider the effect of excited states in the data analysis. In both the Zr^+ and $Zr^+(H_2)_n$ ions, there may be several thermally accessible excited states due to the variety of electronic configurations available to the metal, as well as the variety of available binding sites in the unsaturated clusters. While the reported $\Delta H_0°$ values reported here refer to ground-state products and reactants, the experimentally observed $\Delta H_T°$ and $\Delta S_T°$ may include contributions from excited states. It is straightforward to show that the experimentally observed $\Delta G_{obsd}°$ is related to the true $\Delta G°$ (for ground-state reactants going to ground-state products) by eq 3,

$$\Delta G° = \Delta G_{obsd}° - RT \ln\left[\frac{1 + \sum_i \exp(-\delta G_{R_i}/RT)}{1 + \sum_j \exp(-\delta G_{P_j}/RT)}\right] \quad (3)$$

where the term δG_{P_j} (δG_{R_i}) refers to the free energy difference between the ground state of the product (reactant) cluster and its j^{th} (i^{th}) excited state.

For each observed cluster equilibrium, the best theoretical values for rotational constants, vibrational frequencies, and excited-state free energies are used to try to fit the experimental $\Delta G°$ vs T curves. Often, the calculated and experimental slopes, corresponding to $-\Delta S_T°$, do not agree exactly. Some of the disagreement may be due to mass discrimination in the quadrupole which results in an error in the observed $\Delta S_T°$ equal to $R \times$ ln(mass discrimination). An apparent mass discrimination term, "MD", can thus be calculated and added to the calculation of $\Delta G°$ to match experiment. Ultimately, the calculated rotational constants and vibrational frequencies are varied over wide ranges, while the mass discrimination is adjusted to match the experimental plot. The resulting range of $\Delta H_0°$ is generally less than 0.3 kcal/mol. Errors in temperature measurement propagate in a similar fashion, giving much larger errors in $\Delta S_T°$ than in $\Delta H_0°$. In these experiments, we observed clustering entropies that were on average about 2 cal/(K·mol) more negative than our calculations showed. This is a larger than expected deviation, and may indicate a small systematic error in temperature measurement.

Kinetics. As mentioned above, equilibrium was reached very rapidly for the formation of all clusters after the first; the initial $Zr^+ + H_2 \rightarrow ZrH_2^+$ reaction required a much longer time. This one observation is sufficient to show that this first reaction is not a simple clustering of Zr^+ and an intact H_2 molecule. To help determine what actually occurs in this first addition, we investigated the temperature and pressure dependencies of the forward and reverse reaction rate coefficients. As in our previous work on $Sc^+(H_2)_n$,[5] the slow approach to equilibrium was

modeled assuming a simple bimolecular association mechanism as in eq 4. From this mechanism, the product/parent ion ratio

$$Zr^+ + H_2 \underset{k_b}{\overset{k_f}{\Longleftrightarrow}} ZrH_2^+ \tag{4}$$

is given by eq 5, where R_t is the ratio of ZrH_2^+ to Zr^+ at time t, R_{eq} is the final equilibrium ratio, and $q \equiv k_b + k_f[H_2]$, where $[H_2]$ is the number density of H_2. Both the equilibrium ratio

$$R_t = \frac{R_{eq}(1 - e^{-qt})}{(1 + R_{eq}e^{-qt})} \tag{5}$$

and the concentration of H_2 are known. The backward rate k_b can be determined using k_f and the equilibrium constant using $K_{eq} = k_f/k_b$. There are several corrections to the kinetic data that must be addressed in this analysis: penetration of nascent Zr^+ ions into the reaction cell before becoming thermalized, reducing the reaction time, collision-induced dissociation (CID) of cluster ions between the reaction cell and the detector, and, finally, formation of higher order clusters. The last two effects both reduce the apparent amount of reaction.

When reaction rates are measured within the reaction cell, the amount of time that ions spend in the cell (the reaction time) is varied by changing the electric drift potential. The absolute times are then calculated using the measured ion mobility. Measurement of mobilities is described elsewhere.[33] In these experiments, the absolute mobility was measured as a function of pressure at several temperatures, and was observed to increase slightly at lower pressures (about 7% at the lowest pressures). This is due to ions penetrating into the reaction cell a significant distance before becoming fully thermalized. Fortunately, the effect is small, and simply accounted for by scaling the time axis during the data analysis.

A more important problem in measuring reaction rates is due to CID effects. When measuring equilibrium constants (to determine $\Delta G°$), we can test for CID by repeating the measurement at different pressures. In cases where CID is observed to be an important effect, it tends to scale linearly with pressure. Thus, the true equilibrium constant is taken as the extrapolated value at zero pressure. The earlier equilibrium measurements were performed on a different instrument than that used in the pressure-dependent kinetic studies, and little or no CID was observed at that time. However, CID appeared significant in the more recent kinetic studies. If the true (zero pressure) equilibrium constant is known, it can be used to simply scale the observed equilibrium constant to account for CID. In fact, our present low-pressure data agree well with the previous experiments, and we have used the true equilibrium value to correct for CID in our kinetic data.

One further potential error in our rate determinations is sequential clustering beyond the first addition. These higher clusters are products of the reaction of interest and must be included. As all the observed clusters beyond the first were observed to be in equilibrium at the shortest times in these experiments, we can account for this clustering by summing the first and second clusters (and higher, if present) together to give a "kinetic" product/parent ratio equal to $(ZrH_4^+ + ZrH_2^+)/Zr^+$. This is a very small correction except at the lowest temperatures and highest pressures. The small relative amount of the second cluster also means that ignoring CID of the second cluster should not lead to significant error.

Theoretical Method

All calculations were performed using the GAUSSIAN 94[34] and GAUSSIAN 98[35] program suites. For zirconium, the effective core potential (ECP) of Hay and Wadt[36] was used, which replaces the inner 1s, 2s, 3s, 2p, 3p, and 3d electrons, and incorporates the mass−velocity and Darwin relativistic effects. The basis set used for the valence electrons is a modified contraction of their valence basis.[36] The s basis is constructed from the first three primitive Gaussians making up the 4s orbital, leaving the fourth and fifth primitive Gaussians uncontracted. The p and d bases are treated similarly, leading to a (5s5p4d)/[3s3p2d] contraction scheme, to which we added one additional diffuse d function with an exponent of 0.01. For hydrogen, the scaled (4s)/[2s] basis set of Dunning[37] was used, to which was added a diffuse s (0.071) and two p (1.2 and 0.40) functions.

Geometry optimizations were performed using density functional theory (DFT), specifically the Becke3LYP hybrid functional. A variety of geometries and electronic configurations were considered, and all minima were confirmed by frequency analyses. The B3LYP functional has proven to work well for $M^+(H_2)_n$ clusters for first-row transition metals,[6,7,12,13,19,20] but the lowest energy $Zr^+(H_2)_n$ minima were subsequently reoptimized using MP2 theory to gauge the performance of B3LYP. The binding energy of the first H_2 molecule to Zr^+ was calculated relative to the lowest energy electronic configuration found for Zr^+ using that method ($^4F(4d^3)$ with B3LYP and $^4F(4d^25s^1)$ with MP2). Also, in the present calculations we have considered cluster states in which all H_2 molecules are bound intact (as dihydrogens) as well as forms in which Zr^+ has inserted into one H_2 (dihydrides). Calculating the relative energies of inserted and noninserted forms is challenging, and it is useful to compare results of DFT with more conventional techniques such as MP2. For the noninserted geometries, we also examined both doublet and quartet states (inserted forms result only in doublets within the valence manifold). Although geometries varied very little between the B3LYP and MP2 results, frequency calculations were repeated for the MP2 minima to ensure that true local minima were found. While there is no foolproof method for ensuring that *global* minima were found, care was taken to try all reasonable possibilities, taking into consideration possible electronic configurations as well as ligand arrangements. In this respect, previous calculations on $Ti^+(H_2)_n$ proved useful in formulating a reasonable set of possible structures.[6]

Results and Discussion

The results of the equilibrium experiments will be presented first, followed by the theoretical results. Last, the kinetic results will be presented along with a discussion of their implications for the insertion mechanism of Zr^+ into H_2.

Experimental Results. The experimentally determined $\Delta G°$ vs temperature plots for the sequential clustering reactions of Zr^+ with up to seven H_2 ligands are shown in Figure 1. The lines through the data points are linear least-squares fits with slopes equal to clustering entropies (actually $-\Delta S_T°$) and intercepts equal to clustering enthalpies ($\Delta H_T°$), where T is the average experimental temperature. The fitting of these data with curves from statistical mechanical calculations gives the binding energies at 0 K ($\Delta H_0°$; see the Experimental Method). These quantities are listed in Table 1. The data are quite linear over the temperature range of the experiment as expected. There is slightly more deviation in the first cluster data, possibly due to the fact that equilibrium was reached only at long cell drift times, leading to much lower signal intensities at equilibrium. The first H_2 is also more strongly bound than subsequent ligands, which show a smooth, monotonic decrease in binding energy as

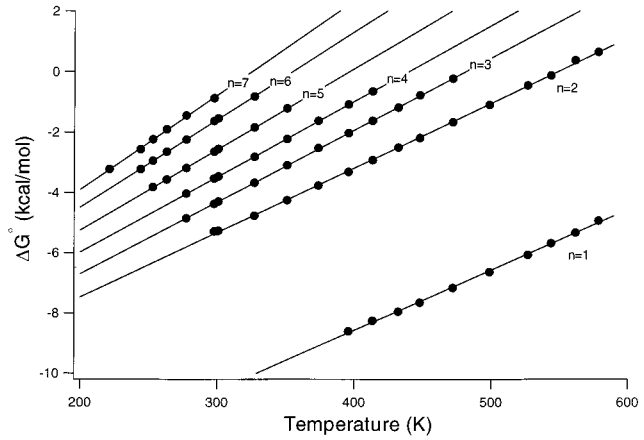

Figure 1. $\Delta G°$ vs temperature for the reaction $Zr^+(H_2)_{n-1} + H_2$ S $Zr^+(H_2)_n$, $n = 1-7$.

TABLE 1: Summary of Experimental Binding Entropies and Enthalpies: $Zr^+(H_2)_{n-1} + H_2 \rightarrow Zr^+(H_2)_n$

n	$\Delta S_T°$[a]	$\Delta H_T°$[b]	$\Delta H_0°$[b]
1	20.2 ± 0.2	16.7 ± 0.1	14.5 ± 0.3
2	21.5 ± 0.1	11.8 ± 0.1	10.7 ± 0.2
3	23.8 ± 0.1	11.5 ± 0.1	10.1 ± 0.3
4	25.0 ± 0.1	11.0 ± 0.1	9.1 ± 0.5
5	26.7 ± 0.2	10.6 ± 0.1	9.2 ± 0.5
6	29.0 ± 0.2	10.3 ± 0.1	8.6 ± 0.6
7	30.4 ± 0.4	9.9 ± 0.1	8.5 ± 0.8

[a] cal/(K·mol). [b] kcal/mol.

subsequent H_2 ligands are added. There is an equally smooth decrease in entropy (increase in $-\Delta S_T°$) with an increase in cluster size.

These binding energies show a trend nearly identical to that of $Ti^+(H_2)_{1-6}$, with two important exceptions. First, for the first-row congener Ti^+, the first H_2 was found to be bound by 2.2 kcal/mol less than the second H_2, and this was attributed to the cost of promotion from the $4s^13d^2$ ground state to the lowest energy $3d^3$ state 2.5 kcal/mol higher in energy. Even single occupation of the large 4s orbital leads to long-range Pauli repulsion with the filled ground state of the incoming H_2 ligand. For Zr^+, the comparable $4d^3$ state is 7.2 kcal/mol above the $5s^14d^2$ ground state, and yet the first H_2 is bound about 4 kcal/mol more strongly than the second H_2. Note also that equilibrium in the first $Ti^+ + H_2$ addition was achieved very quickly, unlike the Zr^+ case. The second difference is that Zr^+ binds seven H_2 ligands within the first solvation shell, while Ti^+ only binds six. This latter difference may not be too surprising since the second-row transition metals are larger than the first-row transition metals, and are known to form higher coordinated species than the first-row transition metals.[38]

Theoretical Results. A summary of low-energy $Zr^+(H_2)_n$ cluster states examined using DFT and found to be local minima (having all real vibrational modes) is given in Table 2. Likewise, the results of MP2 calculations are given in Table 3. (A more complete listing of all local minima found using DFT is given as Supporting Information, including absolute energies, Cartesian coordinates, and frequencies.) No local minima were found at either level of theory for noninserted doublet ZrH_2^+. That is, all attempts at optimizing a noninserted structure for the first cluster spontaneously inserted on the doublet surfaces. Although quartet minima for uninserted $Zr^+(H_2)_n$ clusters were calculated for all but the last (seventh) cluster with DFT, the reliability of comparing doublet and quartet states is questionable, as can be seen by comparing the DFT and MP2 results, which differ significantly for the first cluster. Consequently we will restrict

TABLE 2: Confirmed DFT(B3LYP) Minima: $Zr^+(H_2)_n$

n	sym	state	D_e[c]	D_0[c]
1[a]	C_{2v}	$^2B_1$	16.33	16.62
	C_{2v}	$^2A_1$	16.13	16.47
	C_{2v}	$^2A_2$	12.63	13.22
1[b]	C_{2v}	$^4A_2$	13.62	12.00
	C_{2v}	$^4A_1$	13.57	11.94
	C_{2v}	$^4B_1$	11.95	10.44
2[a]	C_{2v}	$^2B_1$	11.57	8.41
	C_{2v}	$^2B_1$	13.27	8.46
	C_s	$^2A''$	13.41	10.57
2[b]	C_s	$^4A''$	10.83	6.42
3[a]	C_s	^2A	11.09	7.88
	C_s	$^2A''$	11.87	7.87
	C_s	^2A	12.53	7.62
3[b]	C_{3v}	$^4A_1$	10.73	6.03
	C_{3v}	$^4A_1$	10.62	6.05
4[a]	C_s	^2A	4.70	2.81
	C_s	$^2A''$	11.01	8.02
4[b]	C_{4v}	$^2A_1$	13.72	7.64
	C_s	$^4A''$	9.40	6.35
5[a]	C_{2v}	$^2A_1$	5.47	5.47
	C_1	^2A	6.47	5.68
5[b]	C_{2v}	$^2A_2$	9.13	6.97
	C_s	$^4A''$	6.70	6.37
6[a]	C_s	^2A	6.96	4.59
	C_{2v}	$^2B_1$	5.26	2.72
6[b]	C_{2v}	$^2B_2$	11.04	6.62
	C_s	$^4A''$	8.40	7.50
7[a]	C_2	^2A	2.18	0.24
7[b]	C_{2v}	$^2B_2$	8.98	4.99

[a] Inserted (dihydride) cluster. [b] Noninserted cluster. [c] kcal/mol.

TABLE 3: Confirmed MP2 $Zr^+(H_2)_n$ Minima

n	sym	state	D_e[c]	D_0[c]
1[a]	C_{2v}	$^2B_1$	13.75	13.91
	C_{2v}	$^2A_1$	15.21	15.55
	C_{2v}	$^2A_2$	9.45	9.82
1[b]	C_{2v}	$^4A_2$	3.53	1.78
	C_{2v}	$^4A_1$	3.43	1.64
	C_{2v}	$^4B_1$	4.89	5.76
2[a]	C_{2v}	$^2B_1$	13.24	7.90
	C_s	^2A	12.69	9.48
3[a]	C_s	^2A	14.02	9.26
	C_s	$^2A''$	12.39	8.79
	C_s	^2A	12.07	9.00
4[a]	C_{2v}	$^2B_2$	11.81	9.04
4[b]	C_{4v}	$^2A_1$	11.07	4.61
5[a]	C_{2v}	$^2A_1$	11.56	8.09
	C_1	^2A	10.90	7.31
5[b]	C_{2v}	$^2A_2$	10.85	2.88
6[a]	C_1	^2A	12.21	7.58
	C_{2v}	$^2B_1$	9.16	4.51
6[b]	C_{2v}	$^2B_2$	14.11	6.96
	C_s	$^4A''$	7.93	6.46
7[a]	C_2	^2A	7.86	6.23
	C_{2v}	$^2B_1$	7.46	4.46
7[b]	C_s	$^2A''$	11.96	8.88

[a] Inserted (dihydrogen) cluster. [b] Noninserted cluster. [c] kcal/mol.

ourselves to consideration of inserted vs noninserted doublets for the most part. A plot of the binding energies of the lowest energy inserted and noninserted doublets calculated using DFT, together with the experimental values, is shown as a function of ligand number in Figure 2. Figure 3 shows the same binding energies calculated using MP2. The excellent agreement for both methods is striking. Interestingly, both methods predict that a noninserted seventh cluster is favored energetically, although this effect is more pronounced with the DFT calculations, which find the $Zr^+(H_2)_{5-7}$ clusters to all be noninserted, with an especially large difference for the seventh. Both MP2 and DFT methods overestimate the binding energy of the first cluster, but follow the experimental trend in binding energy for the subsequent clusters almost exactly. This is probably due to the difficulty of accurately calculating intra-atomic electronic interactions. Progressive saturation of a transition-metal center tends to "sort out" or distinguish between very nearly degenerate electronic states of the isolated atom. After only a few ligands

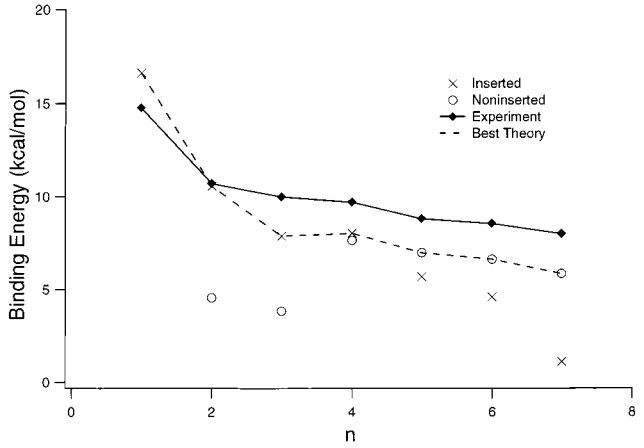

Figure 2. Comparison of experimental binding energies with binding energies calculated using DFT(B3LYP). "Best Theory" refers to the lowest energy doublet state for cluster $Zr^+(H_2)_n$.

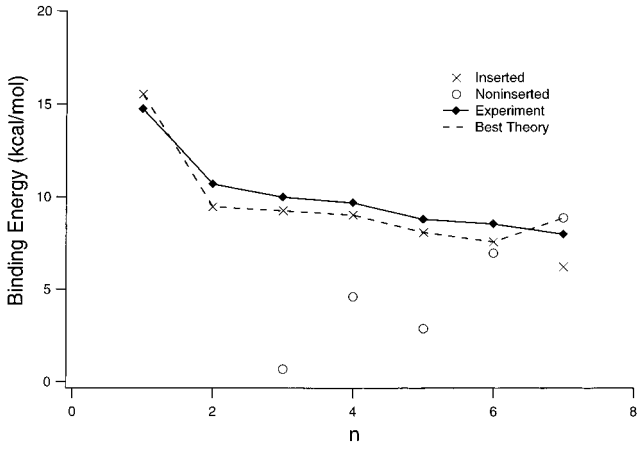

Figure 3. Comparison of experimental binding energies with binding energies calculated using MP2. "Best Theory" refers to the lowest energy doublet state for cluster $Zr^+(H_2)_n$.

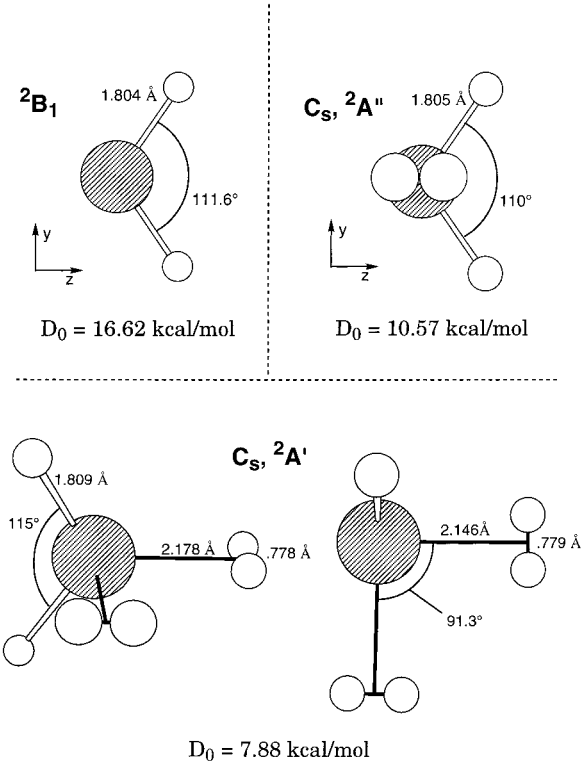

Figure 4. Geometries of the lowest energy doublets found using DFT for $Zr^+(H_2)_{1-3}$.

TABLE 4: NBO Populations for $Zr^+(H_2)_{1,2}$ from DFT

$Zr^+(H_2)_1$	$^2B_1$	$Zr^+(H_2)_2$	$^2A'$
5s	0.302	5s	0.347
$4d_{xz}$	0.996	$4d_{xz}$	0.929
$4d_{yz}$	0.693	$4d_{yz}$	0.715
$4d_{x^2-y^2}$	0.321	$4d_{x^2-y^2}$	0.426
H(1s)	1.346	hydride(1s)	1.346
		hydroge n(1s)	0.997

are added, orbitals tend to become more localized, if only by symmetry, and metal−ligand interactions become more dominant. It is interesting to note the different dependencies that the DFT and MP2 calculations predict for the change in the relative stabilities of the noninserted clusters with cluster size. As *n* increases, the noninserted binding energies rise much more rapidly with MP2 than with DFT (Figures 2 and 3), possibly due to a larger basis set superposition error (BSSE) for MP2. The greater dependence on basis set completeness for MP2 relative to DFT is well-known,[39] and BSSE is a byproduct of using finite basis sets.

The DFT geometries of the lowest energy states for $HZr^+H(H_2)_{1,2}$ are shown in Figure 4. We focus our attention on the density functional structures because of space constraints, and because the MP2 results are in very good agreement with the results of DFT/B3LYP. The first cluster is predicted to be inserted. Two hydrogen atoms are bound to a Zr^+ center that is sd hybridized. The largely hydridic nature of these directly bound hydrogens is evident from the large negative charge density given by a natural bonding orbital (NBO) analysis (see Table 4). MP2 gives a $^2A_1$ ground state rather than a $^2B_1$ state for the HZr^+H system; however, the two states differ only in which nonbonding d orbital on Zr^+ is singly occupied: $d_{x^2-y^2}$ ($^2A_1$) or d_{xz} ($^2B_1$). Neither orbital interacts strongly with the H atoms.

In the second cluster, the dihydrogen approaches the nonbonding singly occupied orbital with the correct symmetry to receive back-donation into the H_2 σ^* orbital. The H−Zr−H bond angle, Zr−H bond length, and orbital occupation are not significantly altered by addition of the H_2 ligand. Insertion into the first H_2 leaves only one valence electron remaining on Zr^+, resulting in a rather unrestrained, flexible bonding environment for subsequent H_2 ligands. H_2 ligands are also able to bind at several possible sites in the earlier unsaturated $HZr^+H(H_2)_n$ clusters, and theory reflects this in several low-lying states found for the second and third clusters (Tables 2 and 3).

The lowest energy third cluster is shown in Figure 4 and is formed by adding a second dihydrogen to $HZr^+H(H_2)$ at a right angle to the first. The zirconium dihydride foundation is still only very slightly perturbed from that of HZr^+H. There seems to be a greater interaction between Zr^+ and the H_2 ligand closer to the hydrides as evidenced by its shorter Zr−H_2 and longer H−H bond lengths. Both DFT and MP2 predict three nearly degenerate structures for inserted $HZr^+H(H_2)_2$, suggesting that there is probably an equilibrium mixture of different structures in our experiment. We cannot experimentally distinguish between these structures, but they have been included in the data analysis described in the Experimental Method.

Figure 5 shows the DFT geometries for the lowest energy inserted $HZr^+H(H_2)_3$ and noninserted $Zr^+(H_2)_4$ clusters. The inserted geometry shows a slight increase in metal−hydride bond length, and decreased metal−dihydrogen bond lengths. The noninserted structure for the fourth cluster is especially favorable, with all four H_2 ligands able to align perfectly for

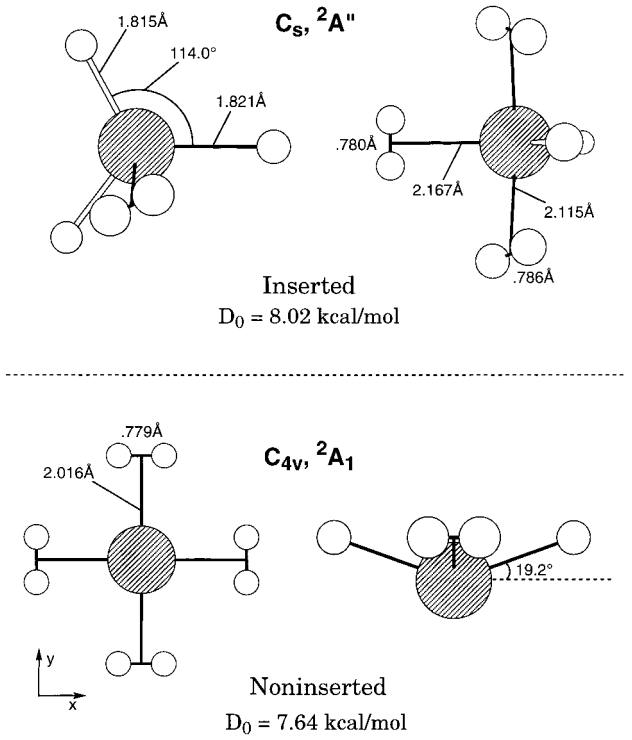

Figure 5. Geometries of the lowest energy inserted and noninserted doublets of $Zr^+(H_2)_4$ using DFT(B3LYP).

back-donation from the doubly occupied d_{xy} orbital (Zr^+ having a $d_{xy}^2d_{z^2}^1$ occupation for the lowest noninserted doublet). Back-donation from doubly occupied d_π orbitals has been seen to be a large factor in determining relative bond strengths for first-row transition-metal/dihydrogen systems, contributing an estimated 6 kcal/mol in bonding to each ligand in such a configuration.[17] The lower relative energy of the fourth noninserted doublet to the third is evident in Figures 2 and 3. However, both DFT and MP2 still predict the ground state of $Zr^+(H_2)_4$ to be inserted. Both methods also show a bending out of plane from the ideal D_{4h} configuration. This could be caused by a repulsive interaction with the singly occupied d_{z^2} orbital, though the origin of this distortion is not fully understood.

Geometries for the lowest energy structures of $HZr^+H(H_2)_4$ and $Zr^+(H_2)_5$ are given in Figure 6. The ground state for the inserted cluster has now lost all symmetry, and the exact shape (and interaction with dihydrogen ligands) of the unpaired metal electron is difficult to describe. The metal−hydride bonds again increase very slightly in the inserted form. On the other hand, the noninserted ground state is well suited to receive back-donation from the doubly occupied d_{yz} orbital. The third valence electron is in the d_{xy} orbital, which can further interact with the two ligands above and below the *yz* plane. Although the metal−H_2 bond distances are slightly longer in this cluster than for $n = 4$, the H−H bond distances are all larger, indicating increased back-donation from the d_π orbitals of Zr^+. The noninserted geometry is in fact now favored in the DFT calculations. Since only one electron is formally available to interact with all the intact H_2 ligands in the inserted clusters, it is not surprising that the noninserted form ultimately binds more strongly than the inserted form as ligation increases.

Figure 7 shows the $HZr^+H(H_2)_5$ and $Zr^+(H_2)_6$ ground-state doublets. The noninserted cluster now has four H_2 molecules well aligned for back-donation from the doubly occupied d_{xy} orbital, and two H_2 molecules are midway between this orbital and the singly occupied d_{yz}, which also has the correct symmetry for back-donation. The inserted cluster has now adopted an

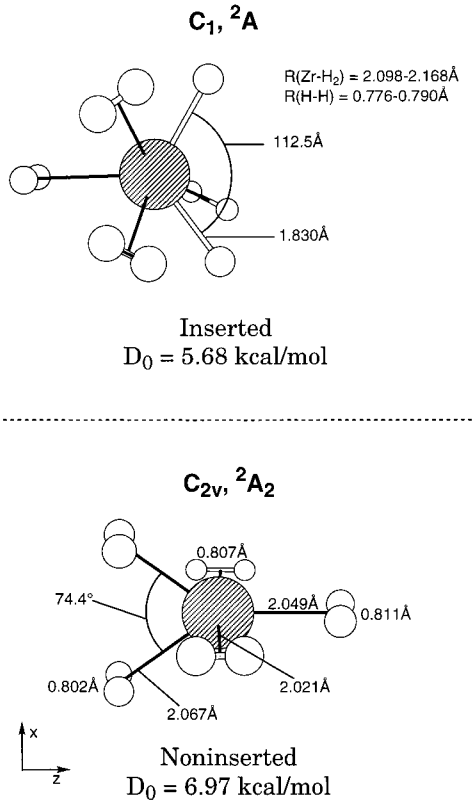

Figure 6. Geometries of the lowest energy inserted and noninserted doublets of $Zr^+(H_2)_5$ using DFT(B3LYP).

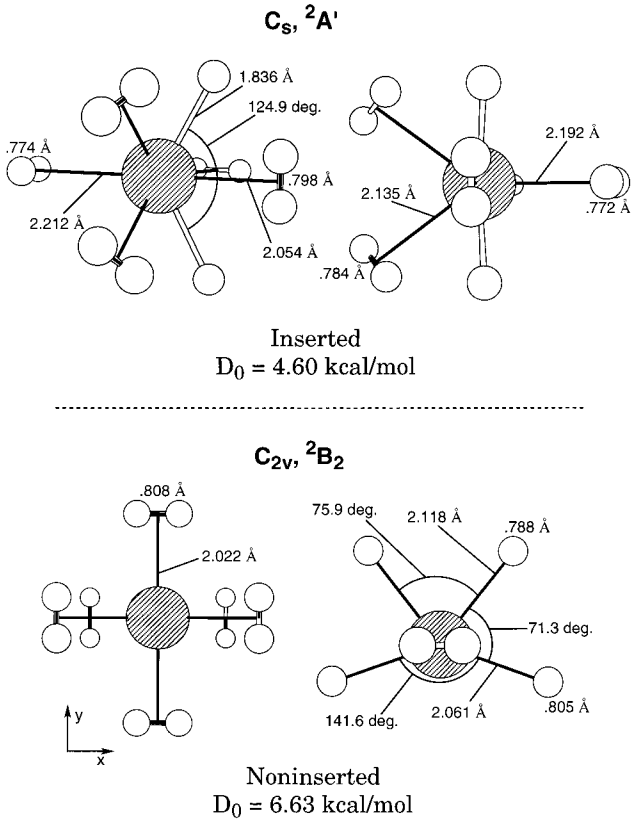

Figure 7. Geometries of the lowest energy inserted and noninserted doublets of $Zr^+(H_2)_6$ using DFT(B3LYP).

interesting conformation with one H_2 ligand almost exactly between the two hydrides. The dihydrogens align themselves with the negatively charged hydrides in several of the calculated

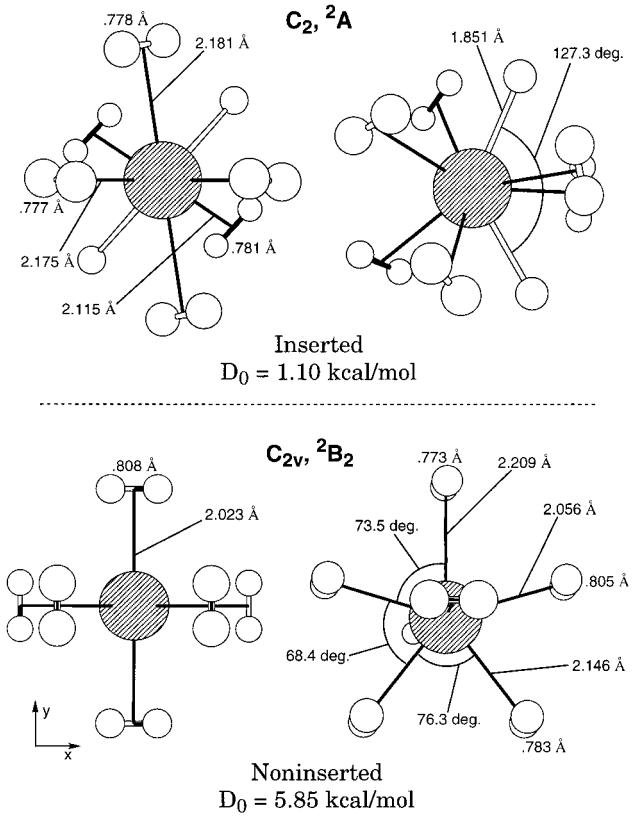

Figure 8. Geometries of the lowest energy inserted and noninserted doublets of $Zr^+(H_2)_7$ using DFT(B3LYP).

inserted $HZr^+H(H_2)_n$ cluster structures, perhaps due to the attractive charge−quadrupole attraction, since H_2 is slightly negatively charged at the dihydrogen bond, and more positively charged on the ends.

Though we have not been considering the quartet clusters, $Zr^+(H_2)_6$ offers the ideal bonding situation for a quartet Zr^+. It is possible to arrange six H_2 molecules around Zr^+ in a pseudooctahedral configuration (actually C_{3v}) in which all dihydrogens approach empty d orbital lobes and are perfectly aligned to received back-donation, albeit from singly occupied d orbitals, which is less favorable due to d−d exchange loss. This Zr^+ state corresponds to the first excited ^{4}F state of Zr^+, which mixes with the ground state (also a ^{4}F state). These factors combine to give a quartet as the ground state of $Zr^+(H_2)_6$ at the DFT/B3LYP level. However, this state is less than 1 kcal/mol below the doublet, and MP2 predicts it to be higher in energy than the doublet. Thus, the spin of the true ground state is unclear.

Figure 8 shows the lowest energy DFT calculated structures for $HZr^+H(H_2)_6$ and $Zr^+(H_2)_7$. The inserted structure has the largest H−Zr−H bond angle of any of the inserted $HZrH^+(H_2)_n$ clusters in the series, and the Zr−H bond lengths are elongated still further. At this point, six dihydrogens must share a single unpaired d electron for any covalent interaction, and the binding energy has dropped significantly from the sixth cluster. The noninserted structure, however, is still able to have four H_2 molecules in a favorable position for back-donation from the doubly occupied d_{xy} orbital, while two others are able to interact weakly with both the d_{xy} orbital and the singly occupied d_{yz} orbital. The seventh H_2 is aligned with the d_{yz} orbital. The H−H bond lengths are seen to decrease in exactly this order, corresponding to their interaction with the Zr^+ valence orbitals.

We are not able to distinguish between inserted and noninserted structures experimentally, but the agreement between

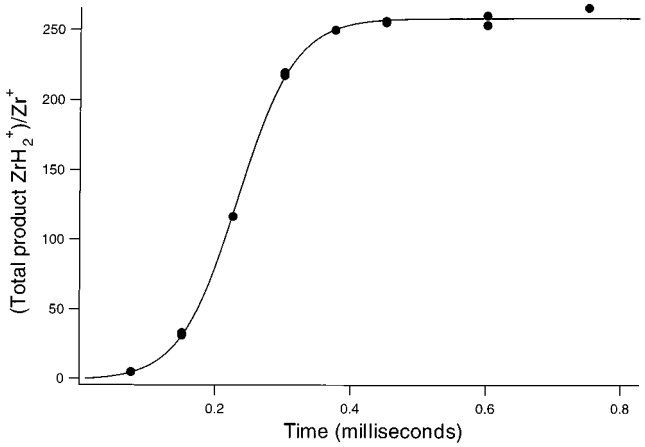

Figure 9. Ratio ZrH_2^+/Zr^+ vs time at 396 K in 3 Torr of H_2. The line corresponds to a fit using eq 5 with $k_f = 3.61 \times 10^{-13}$ cm^3/s.

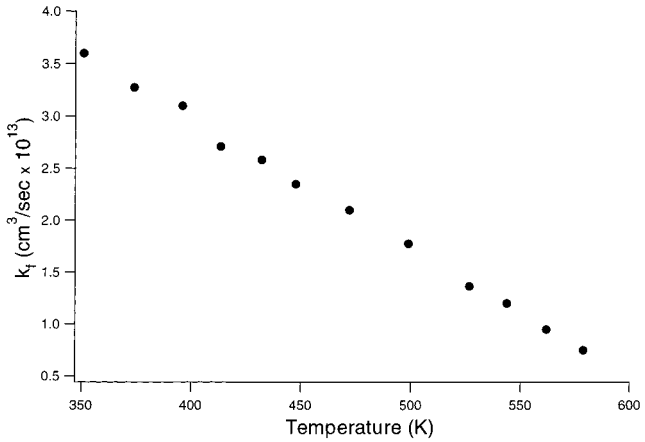

Figure 10. Bimolecular rate constant for formation of ZrH_2^+ vs temperature.

experimental and theoretical binding energies at least suggests that a transition from inserted to uninserted occurs at some point between the fourth and seventh clusters. We see no evidence of a slow reaction leading from inserted to noninserted forms of Zr^+/H_2 clusters, but this is perhaps not surprising given the flexibility of these clusters and the huge phase space present in the larger clusters. In agreement with the DFT calculations, MP2 calculations also predict a noninserted ground state for $Zr^+(H_2)_7$, although the energy difference is smaller and less compelling. There is probably no simple procedure to determine the presence or absence of inserted clusters. Certainly this type of experimental apparatus is unsuitable. However, the possibility that zirconium cations can insert into dihydrogen and then "uninsert" after the addition of six fairly weakly bound ligands demonstrates the delicate balance between different types of bonding in transition-metal systems. Theory certainly suggests that the strong interaction present between Zr^+ and two hydride ligands can be offset by a weaker yet significant interaction spread out over many dihydrogen ligands.

Kinetic Results. Rates were determined as outlined in the Experimental Method. A representative fit of kinetic data using eq 5 is shown in Figure 9. Forward rate coefficients (k_f) were derived from similar fits of kinetic data taken at approximately constant number density over a wide range of temperatures (350−580 K). The results are shown in Figure 10. The rate constant shows a steady negative temperature dependence over the entire temperature range. This dependence is obviously inconsistent with a simple energetic barrier in a bimolecular

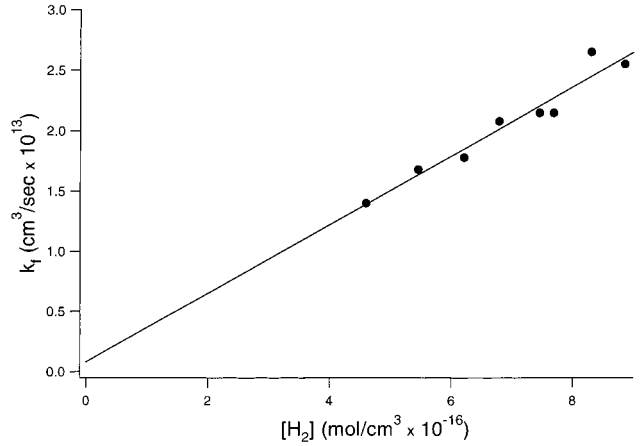

Figure 11. Bimolecular rate constant for formation of ZrH_2^+ vs the number density of H_2. The line represents a linear least-squares fit of the data.

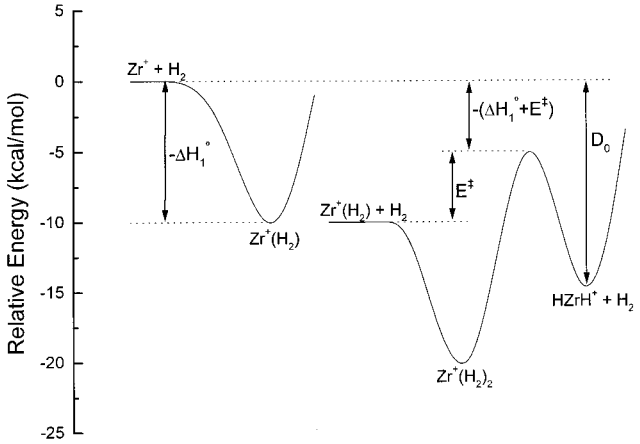

Figure 12. A schematic potential energy surface showing the pertinent quantities for a cluster-assisted reaction mechanism in the reaction of Zr^+ with H_2.

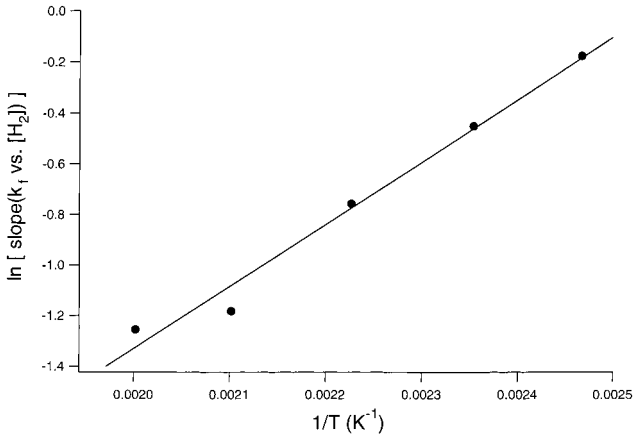

Figure 13. ln(slope of k_f vs N/V) vs $1/T$ from the pressure dependence measurements. The slope is equal to $-(\Delta H_1^\circ + E_1^\ddagger)/R$ (see the text).

reaction pathway. On the other hand, a barrier must be present. Otherwise the reaction would proceed at a rate near the collision rate (about 10 000 times faster than we observe). Further, Das and Balasubramanian[40] have published a theoretical PES for the insertion of Zr^+ into H_2 that shows a barrier of about 12.5 kcal/mol for the ^4F ground state. Unfortunately, their assignment of the ^2P state of Zr^+ to the insertion asymptote at infinite separation is in error. The state with the correct symmetry to insert adiabatically into H_2 is the ^2D state (analogous with the insertion reaction of Sc^+ into H_2).[5,41] This state lies 4.5 kcal/mol below the ^2P state,[42] giving an estimated barrier to insertion from the ground state of about 8 kcal/mol. Again, the observed negative temperature dependence is inconsistent with a simple bimolecular reaction with a barrier this high.

We found a similar paradox in our studies of the insertion reaction of Sc^+ and B^+ into H_2.[5,15] In these systems much higher barriers of about 20 and 77 kcal/mol were predicted,[15,41] and we proposed a cluster-assisted mechanism to explain the anomalous temperature dependencies. In the Sc^+ case, we were unable to experimentally verify this mechanism, although a qualitative analysis of the available excited states, possible surface crossings, and known cluster binding energies showed that it was certainly reasonable. In the $B^+ + H_2$ insertion reaction, an intense theoretical effort was made to examine the insertion barriers in the larger clusters. The results showed that the barrier to insertion decreased from 77 kcal/mol for the bare B^+ ion to ~1 kcal/mol in $B(H_2)_3^+$.[21]

In an attempt to experimentally examine this process more thoroughly, we measured the pressure dependence of the insertion rate coefficient at selected temperatures. The rate coefficient will exhibit a different dependence on H_2 pressure depending on which of the actual $Zr^+(H_2)_n$ uninserted clusters is the actual reactant in the insertion process. Results at 500 K are shown in Figure 11. There is an approximately linear dependence of the rate constant on pressure. Now, in our experiment, noninserted clusters reach equilibrium on a time scale shorter than we can observe. The ratio of cluster to parent ion is given by eq 6 (where ΔG_1° is the free energy of formation

$$\frac{[Zr^+(H_2)]}{[Zr^+]} = [H_2]e^{-\Delta G_1^\circ/RT} \qquad (6)$$

of the *noninserted* cluster). The linear dependence of k_f on P_{H2} thus argues that the first cluster is the most important cluster in the insertion. (The data probably do not rule out some participation of the larger clusters, however.) If we assume that this cluster is the actual reactant in the insertion into H_2, rather than the bare Zr^+ cation, then the apparent rate of insertion from eq 4, k_f, is described by eq 7,

$$k_f \propto [H_2]e^{-\Delta H_1^\circ/RT}e^{-E_1^\ddagger/RT} \qquad (7)$$

where $E_1^\ddagger$ is the barrier of reaction for the first noninserted cluster. Thus, the observed rate is proportional to the pressure of H_2 in the reaction cell, and the temperature dependence is given by the product of exponentials. The reaction will have a negative temperature dependence if the barrier for noninserted $Zr^+(H_2)$ reacting with H_2 is smaller than the binding energy of noninserted $Zr^+(H_2)$. This is shown schematically in Figure 12. This energy difference can be determined by plotting $\ln(k_f/[H_2])$ vs $1/T$, giving a slope of $-(\Delta H_1^\circ + E_1^\ddagger)/R$. The results are shown in Figure 13, and give a value for $-(\Delta H_1^\circ + E_1^\ddagger)$ of 4.9 kcal/mol. If we assume that the first electrostatic cluster is bound by about 10 kcal/mol (we are unable to measure this in our experiment, but it is a reasonable binding energy in analogy to the measured association energies for $Ti^+ + H_2$ and the higher order $Zr^+(H_2)_n$ clusters), the estimated barrier height is about 5 kcal/mol for the insertion of $Zr^+(H_2)$ into H_2. While this energy is approximate, it is reasonable and consistent with a cluster-assisted mechanism that has both a negative temperature dependence and a linear pressure dependence.

Conclusions

We have accurately determined association energies for Zr^+ binding with up to seven H_2 molecules. The first H_2 is bound more strongly, despite the fact that there is a 7.2 kcal/mol promotional cost to reach the first excited $^4F(4d^3)$ state from the more repulsive $^4F(5s^14d^2)$ ground state.[42] This result, together with the relatively slow approach to equilibrium observed for the formation of the first cluster, strongly suggests that insertion into the dihydrogen bond is occurring. After the formation of the first cluster, subsequent binding energies are observed to decrease monotonically up to the seventh cluster, where the first solvation sphere appears to fill. Both DFT(B3LYP) and MP2 calculations are in excellent agreement with the observed trend in binding energies. Both methods indicate that the first cluster is inserted in agreement with our experimental results. Both calculation methods also suggest that the ground state of $Zr^+(H_2)_7$ is actually noninserted, a result we cannot deduce from the experimental data alone. There appears to be a subtle balance between forming strong metal−hydride bonds and more moderate interactions spread among all of the ligands, specifically back-donation from a doubly occupied d_π orbital to H_2 ligands. The calculations show a variety of low-lying structures for $Zr^+(H_2)_n$ clusters due to the flexible three-electron valence shell of Zr^+, similar to that found for $Ti^+(H_2)_n$.

Finally, the reaction kinetics of the first cluster formation were investigated, revealing a negative temperature dependence and a positive pressure dependence of the apparent bimolecular rate constant. Possible explanations for these observations were discussed, and it was shown that both a negative temperature dependence and a positive pressure dependence support a cluster-assisted insertion mechanism wherein noninserted $Zr^+(H_2)$ is the actual reactant that forms the dihydride. These results indicate that further investigation into the pressure dependence of Sc^+ reacting with H_2 may shed light on the mechanism of these fundamental σ bond activation processes.

Acknowledgment. J.E.B. thanks P. Maître for helpful discussions regarding the theoretical calculations performed in this work. The support of the National Science Foundation under Grant CHE-9729146 is gratefully acknowledged. M.T.B. also thanks Aron for his continued inspiration over the past 37 years, starting with his instruction in M.T.B.'s first graduate quantum mechanics class at the University of Illinois. Do you still teach without notes, A.K.?

Supporting Information Available: A listing of all local minima found using DFT(B3LYP) including absolute energies, geometries, and frequencies. This material is available free of charge via the Internet at http://pubs.acs.org.

References and Notes

(1) Kubas, G. J.; Ryan, R. R.; Swanson, B. I.; Vergamini, P. J.; Wasserman, H. J. *J. Am. Chem. Soc.* **1984**, *106*, 451.

(2) Kubas, G. J.; Unkefer, C. J.; Swanson, B. I.; Fukushima, E. *J. Am. Chem. Soc.* **1986**, *108*, 7000.

(3) Chinn, M. S.; Heinekey, D. M. *J. Am. Chem. Soc.* **1987**, *109*, 5865.

(4) Gelabert, R.; Moreno, M.; Lluch, J. M.; Lledós, A. *J. Am. Chem. Soc.* **1998**, *120*, 8168.

(5) Bushnell, J. E.; Kemper, P. R.; Maître, P.; Bowers, M. T. *J. Am. Chem. Soc.* **1994**, *116*, 9710.

(6) Bushnell, J. E.; Maître, P.; Kemper, P. R.; Bowers, M. T. *J. Chem. Phys.* **1997**, *106*, 10153.

(7) Kemper, P. R.; Weis, P.; Bowers, M. T. *Int. J. Mass Spectrom. Ion Processes* **1997**, *160*, 17.

(8) Kemper, P. R.; Bushnell, J.; von Helden, G.; Bowers, M. T. *J. Phys. Chem.* **1993**, *97*, 52.

(9) Bushnell, J. E.; Kemper, P. R.; Bowers, M. T. *J. Phys. Chem.* **1993**, *97*, 11628.

(10) Bushnell, J. E.; Kemper, P. R.; Bowers, M. T. *J. Phys. Chem.* **1995**, *99*, 15602.

(11) Kemper, P. R.; Weis, P.; Bowers, M. T. *Chem. Phys. Lett.* **1998**, *293*, 503.

(12) Weis, P.; Kemper, P. R.; Bowers, M. T. *J. Phys. Chem.* **1997**, *101*, 2809.

(13) Kemper, P. R.; Weis, P.; Bowers, M. T.; Maître, P. *J. Am. Chem. Soc.* **1998**, *120*, 13494.

(14) Bushnell, J. E.; Kemper, P. R.; Bowers, M. T. *J. Phys. Chem.* **1994**, *98*, 2044.

(15) Kemper, P. R.; Bushnell, J. E.; Weis, P.; Bowers, M. T. *J. Am. Chem. Soc.* **1998**, *120*, 7577.

(16) Kemper, P. R.; Bushnell, J.; Bowers, M. T.; Gellene, G. I. *J. Phys. Chem. A* **1998**, *102*, 8590.

(17) Maître, P.; Bauschlicher, C. W., Jr. *J. Phys. Chem.* **1993**, *97*, 11912.

(18) Bauschlicher, C. W., Jr.; Partridge, H.; Langhoff, S. R. *J. Phys. Chem.* **1992**, *96*, 2475.

(19) Bauschlicher, C. W., Jr.; Maître, P. *J. Phys. Chem.* **1995**, *99*, 3444.

(20) Maître, P.; Bauschlicher, C. W., Jr. *J. Phys. Chem.* **1995**, *99*, 6836.

(21) Sharp, S. B.; Gellene, G. I. *J. Am. Chem. Soc.* **1998**, *120*, 7585.

(22) (a) Niu, J.; Rao, B. K.; Khanna, S. N.; Jena, P. *Chem. Phys. Lett.* **1994**, *230*, 299. (b) Kemper, P. R.; Bushnell, J. E.; Maître, P.; Bowers, M. T. *Chem. Phys. Lett.* **1995**, *242*, 244.

(23) Elkind, J. L.; Sunderlin, L. S.; Armentrout, P. B. *J. Phys. Chem.* **1989**, *93*, 3151.

(24) Bauschlicher, C. W.; Langhoff, S. R.; Partridge, H. In *Organometallic Ion Chemistry*; Freiser, B. S., Ed.; Kluwar Academic Publishers: Dordrecht, The Netherlands, 1996; Chapter 2.

(25) Ohanessian, G.; Goddard, W. A., III. *Acc. Chem. Res.* **1990**, *23*, 386.

(26) Armentrout, P. B. *Gas Phase Inorganic Chemistry*; Russel, D. H., Ed.; Plenum Press: New York, 1989.

(27) Bauschlicher, C. W.; Partridge, H.; Sheehy, J. A.; Langhoff, S. R.; Rosi, M. *J. Phys. Chem.* **1992**, *96*, 6969.

(28) Ranasinghe, Y. A.; MacMahon, T. J.; Freiser, B. S. *J. Phys. Chem.* **1991**, *95*, 7721.

(29) Irikura, K. K.; Beauchamp, J. L. *J. Phys. Chem.* **1991**, *95*, 8344.

(30) Perry, J. K. Ph.D. Thesis, California Institute of Technology, Pasadena, CA, 1994, p 78.

(31) Kemper, P. R.; Bowers, M. T. *J. Am. Soc. Mass Spectrom.* **1990**, *1*, 197.

(32) Kemper, P. R.; Hsu, M. T.; Bowers, M. T. *J. Phys. Chem.* **1991**, *95*, 10600.

(33) Kemper, P. R.; Bowers, M. T. *J. Phys. Chem.* **1991**, *95*, 5134.

(34) Gaussian 94, Revision C.2: M. J. Frisch, G. W. Trucks, H. B. Schlegel, P. M. W. Gill, B. G. Johnson, M. A. Robb, J. R. Cheeseman, T. Keith, G. A. Petersson, J. A. Montgomery, K. Raghavachari, M. A. Al-Laham, V. G. Zakrzewski, J. V. Ortiz, J. B. Foresman, J. Cioslowski, B. B. Stefanov, A. Nanayakkara, M. Challacombe, C. Y. Peng, P. Y. Ayala, W. Chen, M. W. Wong, J. L. Andres, E. S. Replogle, R. Gomperts, R. L. Martin, D. J. Fox, J. S. Binkley, D. J. Defrees, J. Baker, J. P. Stewart, M. Head-Gordon, C. Gonzalez, and J. A. Pople, Gaussian, Inc., Pittsburgh, PA, 1995.

(35) Gaussian 98, Revision A.7: M. J. Frisch, G. W. Trucks, H. B. Schlegel, G. E. Scuseria, M. A. Robb, J. R. Cheeseman, V. G. Zakrzewski, J. A. Montgomery, Jr., R. E. Stratmann, J. C. Burant, S. Dapprich, J. M. Millam, A. D. Daniels, K. N. Kudin, M. C. Strain, O. Farkas, J. Tomasi, V. Barone, M. Cossi, R. Cammi, B. Mennucci, C. Pomelli, C. Adamo, S. Clifford, J. Ochterski, G. A. Petersson, P. Y. Ayala, Q. Cui, K. Morokuma, D. K. Malick, A. D. Rabuck, K. Raghavachari, J. B. Foresman, J. Cioslowski, J. V. Ortiz, A. G. Baboul, B. B. Stefanov, G. Liu, A. Liashenko, P. Piskorz, I. Komaromi, R. Gomperts, R. L. Martin, D. J. Fox, T. Keith, M. A. Al-Laham, C. Y. Peng, A. Nanayakkara, C. Gonzalez, M. Challacombe, P. M. W. Gill, B. Johnson, W. Chen, M. W. Wong, J. L. Andres, C. Gonzalez, M. Head-Gordon, E. S. Replogle, and J. A. Pople, Gaussian, Inc., Pittsburgh, PA, 1998.

(36) Hay, P. J.; Wadt, W. R. *J. Chem. Phys.* **1985**, *82*, 299.

(37) Dunning, T. H. *J. Chem. Phys.* **1970**, *53*, 2823.

(38) Cotton, F. A.; Wilkinson, G. *Advanced Inorganic Chemistry*, 2nd ed.; Wiley: New York, 1966; Chapter 30.

(39) Dargel, T. K.; Hertwig, R. H.; Koch, W.; Horn, H. *J. Chem. Phys.* **1998**, *108*, 3876.

(40) Das, K. K.; Balasubramanian, K. *J. Chem. Phys.* **1989**, *91*, 2433.

(41) Rappé, A. K.; Upton, T. H. *J. Chem. Phys.* **1986**, *85*, 4400.

(42) (a) Moore, C. E. *Atomic Energy Levels*; U.S. National Bureau of Standards: Washington, DC, 1952; Vol. Circ. 467. (b) Sugar, J.; Corliss, C. *J. Phys. Chem. Ref. Data* **1978**, *7*, 1194.